## PAPER

# Enhanced bone regeneration by osteoinductive and angiogenic zein/whitlockite composite scaffolds loaded with levofloxacin†

Xue Lin,[a] Yu Wang,[ab] Lingyu Liu,[ab] Xiaomeng Du,[a] Wenying Wang,*[a] Shutao Guo, [c] Jinchao Zhang, [a] Kun Ge*[a] and Guoqiang Zhou [*ab]

Promoting angiogenesis following biomaterial implantation is essential to bone tissue regeneration. Herein, the composite scaffolds composed of zein, whitlockite (WH), and levofloxacin (LEVO) were fabricated to augment bone repair by facilitating osteogenesis and angiogenesis. First, three-dimensional composite scaffolds containing zein and WH were prepared using the salt-leaching method. Then, as a model antibiotic drug, the LEVO was loaded into zein/WH scaffolds. Moreover, the addition of WH enhanced the adhesion, differentiation, and mineralization of osteoblasts. The zein/WH/LEVO composite scaffolds not only had significant osteoinductivity but also showed excellent antibacterial properties. The prepared composite scaffolds were then implanted into a calvarial defect model to evaluate their osteogenic induction effects *in vivo*. Micro-CT observation and histological analysis indicate that the scaffolds can accelerate bone regeneration with the contribution of endogenous cytokines. Based on amounts of data *in vitro* and *in vivo*, the scaffolds present profound effects on improving bone regeneration, especially for the favorable osteogenic, intensive angiogenic, and alleviated inflammation abilities. The results showed that the synthesized scaffolds could be a potential material for bone tissue engineering.

## 1. Introduction

Bone tissue engineering has attracted increasing attention from scientists and the public recently. The damaged parts of natural hard tissue are regenerated through bone remodeling, thus maintaining a healthy state throughout life.[1,2] The scaffolds are essential in forming three-dimensional structures that promote cell adhesion, proliferation, and differentiation. This is attributed to their properties of personalized customization and high precision.[3,4] The formation of new bone depends on the proliferation and differentiation of seed cells migrating from surrounding tissue to the defective area.[5] Recovering large-scale bone defects is a severe clinical challenge for patients and orthopedic surgeons.[6] The vascularization process is a crucial factor in the regeneration of bones on a large scale. A microchannel structure may induce the formation of basic vasculature by endothelial cells.[7] Therefore, developing bone repair

materials with the ability of osteoinductive and angiogenesis is necessary. In addition, postoperative infection is a major risk factor for bone repair surgery, often resulting in severe pain and implant failure.[8] Implants during surgical treatment have no sustained antibacterial effect during bone regeneration. Therefore, the antibacterial properties of implants are key factors in preventing infection.[9]

The second most common inorganic substance in human bones is whitlockite (WH, $Ca_{18}Mg_2(HPO_4)_2(PO_4)_{12}$), which has the same space group as β-tricalcium phosphate.[10] The formation process involves partially substituting calcium ions within the crystal lattice of calcium orthophosphate with magnesium ions.[11] The content of whitlockite is higher than that of hydroxyapatite (HAP) in the early stage of biological mineralization. It is involved in the initial phase of bone regeneration by stimulating osteogenic differentiation and inhibiting osteoclast activity. Synthetic whitlockite nanoparticles can release $PO_4^{3-}$ and $Mg^{2+}$ under physiological conditions and convert them into hydroxyapatite, which actively participates in bone remodeling.[12,13] Protein-based biodegradable composites have widely used in biomedical applications due to their excellent biocompatibility, especially those with components similar to the extracellular matrix.[14,15] There are many studies on zein-based materials for drug delivery and tissue engineering.[16,17] Three-dimensional zein scaffolds with optimal mechanical properties and porous structure are suitable for facilitating cellular migration and tissue proliferation. It is biodegradable and can

[a]*Key Laboratory of Medicinal Chemistry and Molecular Diagnosis of Ministry of Education, Key Laboratory of Chemical Biology of Hebei Province, College of Chemistry and Materials Science, Hebei University, Baoding, 071002, China. E-mail: wzwenying@163.com; kaqikun@163.com; zhougq1982@163.com*

[b]*College of Basic Medical Science, Hebei University, Baoding, 071000, P. R. China*

[c]*Key Laboratory of Functional Polymer Materials of Ministry of Education, State Key Laboratory of Medicinal Chemical Biology, College of Chemistry, Nankai University, Tianjin, 300071, China*

† Electronic supplementary information (ESI) available. See DOI: https://doi.org/10.1039/d4ra00772g

form blood vessels inside the scaffolds.[18,19] Levofloxacin hydrochloride (LEVO) was selected as a model antibiotic drug for loading into zein/WH composite scaffolds due to its established reputation as a fluoroquinolone having broad-spectrum action against Gram-positive and Gram-negative bacteria.[20] The inorganic phases in composite scaffolds can improve the hydrophilicity of the zein matrix and create a suitable environment for cell attachment, spread, and proliferation.[21]

In this study, we fabricated mesoporous zein/WH composite scaffolds loaded with LEVO by salt leaching. The bioactivity, biocompatibility, and antibacterial effects of synthetic scaffolds were evaluated *in vitro*. Furthermore, the bone regeneration effects of composite scaffolds were investigated in the SD Rats skull defect model (Fig. 1). Based on *in vitro* and *in vivo* studies, the scaffolds exhibited profound effects on promoting bone regeneration, especially for the favorable osteogenic, intensive angiogenic, and alleviated inflammation abilities. More interestingly, the scaffolds almost completely healed the defects in rat skulls within six weeks, as revealed by micro-CT imaging and histological analysis.

## 2. Materials and methods

### 2.1. Materials, cell culture and animal model

Sodium dihydrogen phosphate dihydrate ($NaH_2PO_4 \cdot 2H_2O$), anhydrous calcium chloride ($CaCl_2$), sodium chloride (NaCl), and magnesium chloride hexahydrate ($MgCl_2 \cdot 6H_2O$) were bought from Energy Chemical Reagent (Shanghai, China). Levofloxacin hydrochloride (LEVO) was attained from National Institutes for Food and Drug Control (Beijing, China). Zein

(purity > 98%) was bought from J&K Scientific Ltd (Beijing, China). Dimethyl sulfoxide (DMSO), 3-(4,5-dimethylthiazol-2-yl)-2,5-diphenyltetrazolium bromide (MTT), dexamethasone, alizarin red-S (ARS), cetylpyridinium chloride, β-glycerophosphate, penicillin, streptomycin, ascorbic acid was purchased from Sigma-Aldrich Co. (St Louis, MO, USA). Minimum Essential Medium Alpha Medium (α-MEM), High Glucose Dulbecco's Modified Eagle Medium (HG-DMEM), fetal bovine serum (FBS), Hoechst, actin green, and trypsin was obtained from Thermo Fisher Scientific (Waltham, MA, USA). The alkaline phosphatase (ALP) kit was purchased from the Nanjing Jiancheng Biological Engineering Institute (Jiangsu, China). Growth factor reduced Matrigel was acquired from BD Biosciences (San Jose, CA, USA). The mouse osteoblast precursor MC3T3-E1 cells and Human umbilical vein endothelial cells (HUVECs) were acquired from China Infrastructure of Cell Line Resources (Beijing, China). Spraguee-Dawley (SD) rats were attained from Beijing Vital River Laboratory Animal Technology Co., Ltd (Beijing, China).

### 2.2. Preparation of whitlockite

The whitlockite was synthesized according to the modified procedure reported in the previous literature.[22] Aqueous solutions of $CaCl_2$ (100 mM) and $MgCl_2$ (100 mM) in volumes of 7 mL and 3 mL, respectively, were combined with a 10 mL solution of creatine phosphate (60 mM) and poured in 20 mL of deionized water dropwise. The resulting mixture was stirred at ambient temperature using a magnetic stirrer. The solution obtained from the reaction was loaded into a cylindrical
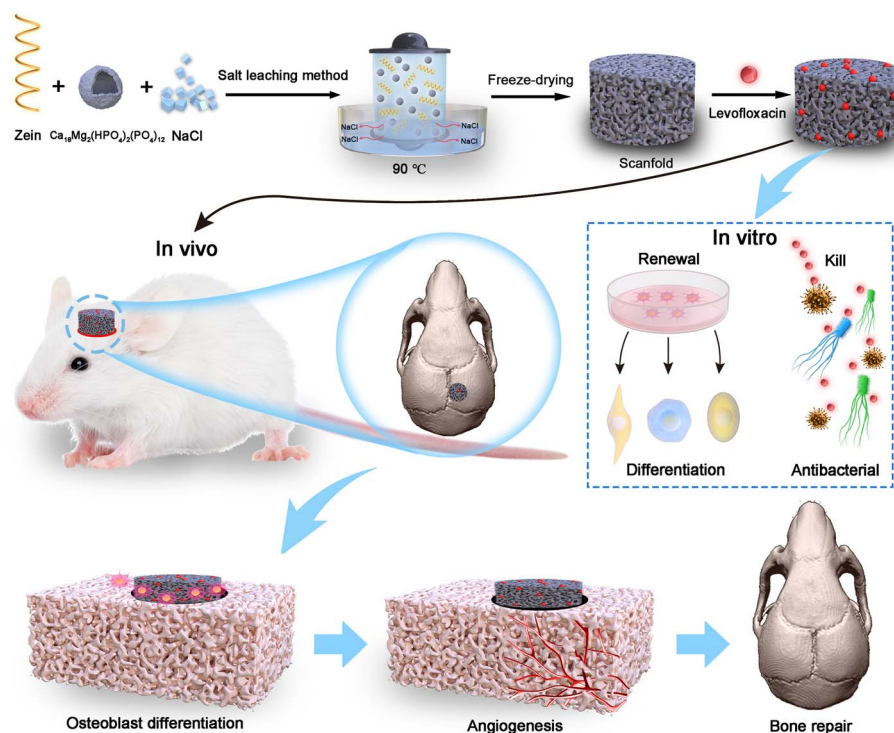


Fig. 1 Synthesis process of the composite scaffolds and mechanism of synergistic bone repair.

autoclave made of polytetrafluoroethylene (100 mL). The autoclave was then sealed and positioned inside a robust external container. After that, the container was heated in a microwave synthesizer (XH-800s, Xianghu, China) to 120 °C and maintained for 10 minutes. The microwave synthesizer is a system for microwave-hydrothermal synthesis that can operate in a continuous heating mode at a frequency of 2.45 GHz and a maximum power of 1000 W. The temperature of the reaction system was measured by a platinum resistance temperature sensor and controlled by microwave power regulation. To achieve relatively uniform heating, the autoclave underwent continuous rotation during the process of microwave irradiation. Upon reaching ambient temperature, the resultant substances were isolated through centrifugation, subjected to multiple rounds of cleansing with deionized water and ethanol, and desiccated at 80 °C for 24 hours.

### 2.3. Preparation of zein/WH/LEVO scaffolds

Zein, WH, and sodium chloride with different particle sizes (150–250 μm) were mixed in certain mass fractions (Zein : WH = 9 : 1, Zein NaCl = 1 : 1.4, w/w). The composite scaffolds made of zein/WH were formed by molding the mixture into three-dimensional structures, then leaching in a water bath at 90 °C for 1 hour and lyophilization for 8 hours.[23] The scaffolds containing 5 mg of zein and WH were immersed in 3 mL of aqueous solution with a concentration of 0.5 mg mL$^{-1}$ LEVO. The mixture was then stirred at room temperature for 24 hours at a speed of 800 rpm. The mixed reaction solution was centrifuged and dried to obtain zein/WH/LEVO scaffolds. The content of LEVO in supernatants was determined by the UV-vis absorption at a wavelength of 290 nm. The drug loading efficiency (LE%) and encapsulation efficiency (EE%) were determined using the following formula separately: LE (%) = ($m_{\text{total levo}}$ − $m_{\text{levo in supernatants}}$)/($m_{\text{total levo}}$ − $m_{\text{levo in supernatants}}$ + $m_{\text{zein/WH}}$) × 100, EE (%) = ($m_{\text{total levo}}$ − $m_{\text{levo in supernatants}}$)/$m_{\text{total levo}}$ × 100. The standard curve for calculating LE% and EE% was provided in the ESI (Fig. S1).†

### 2.4. Characterization of the samples

X-ray powder diffraction (D8 Advance, Bruker, Germany) was used to identify the crystalline phase of synthetic WH. The $2\theta$ angle was varied from 10 to 45°. A specific surface area and pore size analyzer (V-sorb 2800P, Gold APP, China) were used to measure the Brunauer–Emmett–Teller (BET) specific surface areas and pore size distributions of WH. A field emission scanning electron microscope (JSM-7500F; JEOL, Japan) was used to examine the shape and size of WH, zein, zein/WH, and zein/WH/LEVO scaffolds. Using energy-dispersive X-ray spectroscopy (EDS, PhenomProX, Netherlands Phenom-World, Netherlands), the elemental analysis of created samples was examined. With a UV-vis spectrophotometer (UV-2300, Techcomp, China) operating at a wavelength of 290 nm, the LEVO drug concentrations were analyzed. Using a synchronous thermal analyzer (STA409PC, Netzsch, Germany) with a heating rate of 10 °C min$^{-1}$ in flowing air, thermo gravimetric (TG) curves of composite scaffolds were measured. A material testing device (HZ-1007C, Heng Zhun, China) tested the tensile characteristics of scaffolds. Contact angle measurements (OCA 15EC, DataPhysics, Germany) were used to examine the hydrophilicity of composite scaffolds. The scaffolds were cut into a size of 1 mm × 1 mm and glued to the glass slide. 2 μL distilled water was dripped from syringe on the scaffolds and adhered to the slide, then, the contact angle was detected at different time points.

### 2.5. Cell viability assay

A cell incubator (Model MCO-18AIC; Sanyo, Japan) was used to culture MC3T3-E1 and HUVEC cells in α-MEM and HG-DMEM, respectively, cultured in a humidified atmosphere at 37 °C, supplemented with 10% FBS and 1% penicillin/streptomycin. The effects of zein, zein/WH, and zein/WH/LEVO scaffolds on cell viability were tested by the MTT assay. The experimental procedure involved seeding cells onto composite scaffolds at a density of $2 \times 10^4$ cells per ml in 96-well tissue culture plates. This was followed by incubation for 1 and 3 days, then evaluated by the MTT method. The absorbance was measured at a wavelength of 570 nm, utilizing a microplate spectrophotometer (Model 3550, BioRad, USA). The cell viability (%) was calculated according to the formula OD$_{\text{sample}}$/OD$_{\text{control}}$ × 100. For cell spreading and attachment experiments, MC3T3-E1 cells were stained with actin green and Hoechst at 1 and 3 days. The control group was comprised of cells that were cultured on the plate in the absence of composite scaffolds.

### 2.6. ALP activity assay

MC3T3-E1 cells were grown in α-MEM with osteogenic differentiation medium (OS) containing 5 mM β-glycerophosphate, 100 μg mL$^{-1}$ ascorbic acid, and 100 nM dexamethasone. Cells were seeded on composite scaffolds at $2 \times 10^4$ cells per ml density in 24-well plates. Following a 10 days period of cell seeding, the plates underwent a washing procedure utilizing PBS and were subsequently lysed for pyrolysis liquid analysis. Then the expression level of ALP was measured with an ALP kit according to the operating instructions. The measurement of cellular protein content was obtained by micro BCA protein assay kit. Normalization of each value was carried out with respect to the total protein content. The cells cultured with osteogenic differentiation medium were used as a control.

### 2.7. Mineralized matrix formation assay

MC3T3-E1 cells were seeded on different composite scaffolds at $2 \times 10^4$ cells per ml density in 24-well plates with osteogenic differentiation medium. Following a 21 days culture period, the cells were washed twice with PBS and subsequently fixed with 95% ethanol for 10 minutes. After the fixation, the cells were washed with PBS and incubated with 0.1% ARS solution at 37 °C for 30 minutes. Quantitative determination of ARS staining was performed using 10% (w/v) cetylpyridinium chloride elution at ambient temperature for 10 minutes, followed by measurement of absorbance at 570 nm. The cells cultured with osteogenic differentiation medium were used as a control.

## 2.8. Angiogenesis assay

Individual scaffolds weighing 1 gram were submerged in 10 mL of HG-DMEM supplemented with 2% FBS, 100 U mL$^{-1}$ of penicillin, and 100 mg mL$^{-1}$ of streptomycin for 10 days. The (HUVECs) underwent a period of starvation in (HG-DMEM) containing 1% (FBS) for the duration of one night. The conditioned medium for the prepared (HUVECs) was collected on day 10 to inspect the angiogenic potential. A mixture of Matrigel and conditioned medium in a 1 : 1 ratio (v/v) was dispensed into a 24-well plate and subsequently incubated for 1 hour. After that, $2.5 \times 10^5$ cells per well were seeded onto the Matrigel surface, followed by an 8 hours culture period. The tube network was quantified by angiogenesis analyzer for Image J through a random selection of microscope images.[24]

## 2.9. Antibacterial test

The antibacterial activity was evaluated by the agar disc diffusion technique. The antibacterial effect assay used Methicillin-resistant *Staphylococcus aureus* (MRSA) strains. The microorganisms' inoculum was obtained from broth cultures that comprised 0.6% yeast extract and were incubated at a temperature of 37 °C. The agar diffusion assay was executed by carefully pouring agar medium into sterile Petri dishes, allowing for the formation of uniform layers with a thickness of 4 mm. The inoculum was measured at OD$_{600}$ and adjusted to the concentration used in the antibacterial test. Bacterial cultures of MRSA were spread evenly on scaffolds with applicator sticks at a concentration of $5 \times 10^7$ CFU mL$^{-1}$. The bacteria that had been diluted were applied onto a Petri dish, after which the scaffolds were affixed and subjected to incubation at 37 °C for 24 hours. The antibacterial efficacy was assessed by quantifying the area of growth inhibition surrounding the scaffolds.

## 2.10. *In vivo* bone repair effect evaluation

The study involved conducting *in vivo* experiments on male Sprague-Dawley (SD) rats that were 8 weeks old and procured from Beijing Vital River Laboratory Animal Technology Co., Ltd. General anesthesia was initiated through intraperitoneal administration of a mixture containing 1% pentobarbital sodium solution at a dosage of 40 mL kg$^{-1}$. The animals were maintained under general anesthesia throughout the surgical procedure. The cranial hair of the rats was removed, and the area was disinfected with iodophor and 75% ethanol. Calvarial defect model was created by trephine in each rat. Rats were randomly divided into four groups: Control, zein, zein/WH, and zein/WH/LEVO scaffolds. 6 rats were used in each group experiments. The rats with skull defect without scaffolds treatment were used as the control group. The rats were subjected to micro-CT examination within a period of 2–6 weeks during the process of bone regeneration. After 6 weeks, the animals were sacrificed to gather tissue samples. The specimens underwent fixation in neutralized buffered formalin at a concentration of 10% for 24 hours at ambient temperature and were subsequently made ready for analysis *via* micro-CT (μCT). Each specimen was scanned perpendicular to the long bone axis covering the whole calvarium defect. Three-dimensional reconstruction of the cylindrical region of interest was performed using MicView software to quantify the newly formed mineralized tissue. All animal procedures were performed in accordance with the guidelines for care and use of laboratory animals of Hebei University and approved by the Animal Welfare and Ethics Committee of Hebei University (Approval No. IACUC-2018011).

## 2.11. Histological analysis

The specimens were treated with RapidCal™ solution (BBC Chemical Co., Stanwood, WA, USA) to remove calcium and then underwent dehydration using a graded series of ethanol solutions ranging from 70% to 100%. Finally, specimens were paraffin-embedded. Finally, the implant and specimens were sliced into 5 μm thick bone-perpendicular slices. The slides were stained by Hematoxylin and Eosin (H&E) staining, Masson staining and immunohistochemistry (CD31, VEGF) with routine techniques. The antibodies used in immunohistochemistry are rabbit monoclonal [EPR17259] to CD31 and mouse monoclonal [VG-1] to VEGFA, respectively.

## 2.12. Statistical analysis

Data were presented in the form of mean ± standard deviation. All experiments were carried out at least three times independently. The Student's *t*-test was used to analyze the statistics of two groups, and the one-way ANOVA processed the statistics of three or more groups. The significant difference was defined as $P$ values less than 0.05.

# 3. Results and discussions

## 3.1. Characterizations of whitlockite

The WH was prepared as previously described and fed into the bone repair composite scaffolds.[22] The physicochemical properties of phosphates, such as chemical composition, surface morphology, and porosity, are closely related to their biocompatibility, bone conductivity, and bone inductivity.[25] The SEM and TEM results showed that the WH was hollow and particle size was about 950 nm (Fig. 2A and B). Furthermore, the WH is composed of O, P, Mg, and Ca elements, which are likewise dispersed in the WH hollow porous microspheres (Fig. 2C and E). As a representative phosphate, WH contains magnesium ions in its crystal lattice. Magnesium is the fourth most abundant element in the body. It is essential to maintain the balance of mineralized tissues in living organisms and prevent osteoporosis and other bone tissue damage.[26] Compared with pure hydroxyapatite, magnesium ion doping can improve the bone inductivity of hydroxyapatite by increasing the expression of alkaline phosphatase, type I collagen, and VEGF protein, enhancing cell viability and promoting angiogenesis.[27,28] The XRD patterns of WH are shown in Fig. 2D. The main phase of WH, which belonged to the space group $R3c$ (161), was identified as the hexagonal crystal phase (JCPDS No. 00-042-0578). The synthesized powders exhibited diffraction peaks characterized by high intensity and sharpness. No other diffraction
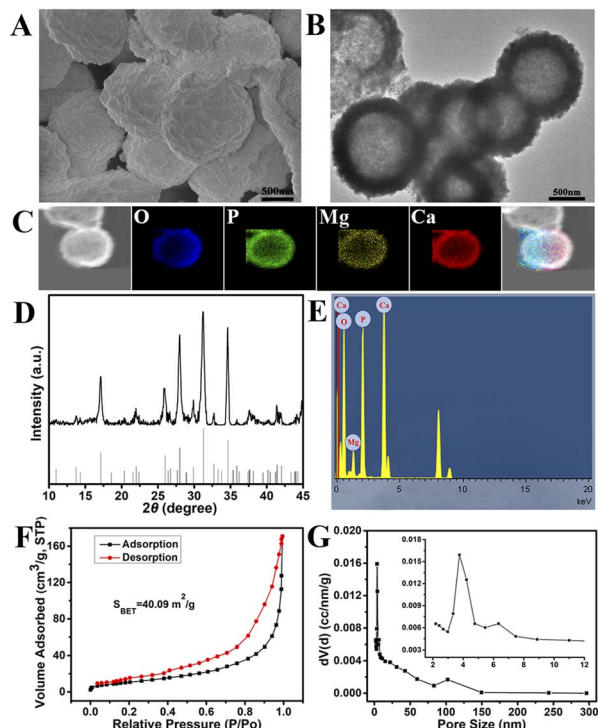
Fig. 2 Characterizations of whitlockite hollow porous microspheres. (A) SEM images; (B) TEM images; (C) the mapping; (D) XRD spectra; (E) elements analysis; (F) nitrogen adsorption–desorption isotherm; (G) pore size distribution.

peaks were found in the spectra. The result indicated that WH particles synthesized have relatively high crystallinity. The results of nitrogen adsorptions–desorption isotherm and pore size distributions showed that the specific surface area and pore size distributions of WH hollow porous microspheres were 40.09 m$^2$ g$^{-1}$ and 3.18 nm, respectively (Fig. 2F and G).

## 3.2. Characterizations of composite scaffolds

The surface of the scaffolds was rough, and the pores of the scaffolds were inhomogeneous (Fig. 3A). The white powders on the surface of scaffolds are WH (Fig. 3B and C). The P, Mg, and Ca elements were observed in zein/WH scaffolds (Fig. 3D and E). F element was observed after mixing with LEVO in the zein/WH scaffolds (Fig. 3F). The results indicated that the zein/WH/LEVO composite scaffolds had been prepared successfully. The UV-visible absorption spectra of LEVO exhibit a characteristic peak at approximately 290 nm, as depicted in Fig. 3G. When the initial concentration of LEVO is 0.5 mg mL$^{-1}$, the loading rate is 10%, and the encapsulation efficiency is 37%, which can be calculated from the standard concentration curve of LEVO. The conclusion was further supported by the thermogravimetric (TG) analysis (Fig. 3H). It also proved that we successfully prepared the zein/WH scaffolds. The tensile strength of three prepared scaffolds was investigated. The stress–strain curves show that the average tensile strength of the zein scaffolds was 21.44 ± 2.35 MPa. After deposition of WH, the tensile strengths of the zein/WH and zein/WH/LEVO scaffolds increased to 28.87
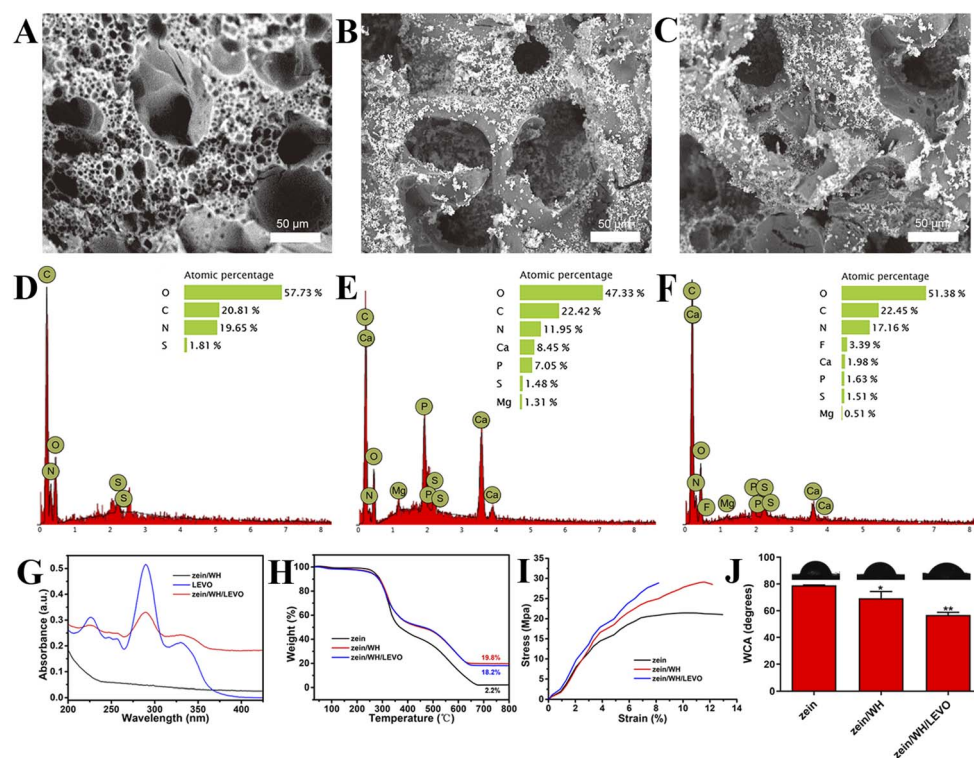


Fig. 3 Characterizations of different scaffolds. (A–C) The scanning electron micrographs of zein, zein/WH and zein/WH/LEVO scaffolds, respectively; (D–F) the elements analyses of zein, zein/WH and zein/WH/LEVO scaffolds, respectively; (G) the UV-vis absorption spectra; (H) the TG curves; (I) the stress–strain curves; (J) the contact angle analysis. *$p < 0.05$ and **$p < 0.01$ for zein/WH, zein/WH/LEVO vs. zein group.

± 2.53 and 29.12 ± 3.06 MPa, respectively (Fig. 3I). The deposition of WH nanoparticles enhanced the tensile properties of zein scaffolds significantly. Previous study has shown that the incorporation of hydroxyapatite nanoparticles into zein can improve the mechanical properties of scaffolds.[29] This may be due to the crosslinking density, electrostatic interactions or hydrogen bonding between inorganic compounds and zein. These results indicate that the zein/WH/LEVO and zein/WH scaffolds have almost the same tensile strength.

The static water contact angle (WCA) analysis was employed to investigate the hydrophilic nature of various scaffolds. The WCA of zein scaffolds is 79.1 ± 0.8°. After blending with WH, the WCA of zein/WH scaffolds decreases to 68.43 ± 5.3° (Fig. 3J). It indicated that the inorganic phase improved the hydrophilicity of the zein matrix, thus providing a suitable environment for cell attachment, spreading, and proliferation. In physiological conditions, the inorganic component WH would gradually convert into hydroxyapatite, which is similar to the main component of bone, and participate in the remodeling process of bone.[30] The zein, which has excellent biocompatibility, degradability, and antioxidant properties, was assembled onto the scaffolds to provide a frame structure.[31] The new bone formation was significantly enhanced with the increase of zein content in the nano magnesium silicate/zein/poly(caprolactone) ternary composites scaffolds.[32] Zein exhibits a suitable porous architecture and mechanical characteristics that are favorable to cellular adhesion, migration, proliferation, and tissue ingrowth.[33] Furthermore, the WCA of the zein/WH/LEVO composite scaffolds decreased to 58.43 ± 2.7°, demonstrating the hydrophilicity of scaffolds could be improved by adsorbing levofloxacin.

## 3.3. The viability and differentiation of MC3T3-E1 cells

Bone repair is a complex dynamic process involving many cells and molecules. To achieve an effective repair effect, it is required to make osteogenic differentiation of stem cells, promote vascular regeneration, and reduce the immune rejection of tissues.[34] Zein has been extensively utilized in the pharmaceutical and biomedical domains, which include drug targeting, tissue engineering, and gene delivery.[35] In previous studies, the addition of zein was reported to enhance the cell adhesion, growth, and proliferation of composite scaffolds.[36] The hydroxyapatite/zein composite membrane can promote the adhesion, proliferation and osteogenic differentiation of mouse bone marrow mesenchymal stem cells.[37] Studies indicated that the cells can attach to the pore walls of zein/chitosan/nanohydroxyapatite scaffolds.[38] The cell response to different scaffolds is examined *in vitro*. Early cell culture adhesion and spreading on scaffolds may affect cell proliferation and directional differentiation. The scaffolds had increased cell viability after 1 and 3 days than the control group (Fig. 4A). The results indicate that three scaffolds have high biocompatibility without appreciable toxicity. As an early marker of osteogenesis, ALP is mainly expressed from 7 to 14 days during the cell culture. The ALP activity of cells cultured on different scaffolds substantially increased with the culture period than that of the control group (Fig. 4B). Therefore, it is indicated that three scaffolds can promote the expression of ALP. Alizarin red staining is utilized to detect cellular mineralization as a late marker of osteogenic differentiation, typically within a culture period of up to 21 days. The quantitative results of staining extracts showed that the cell
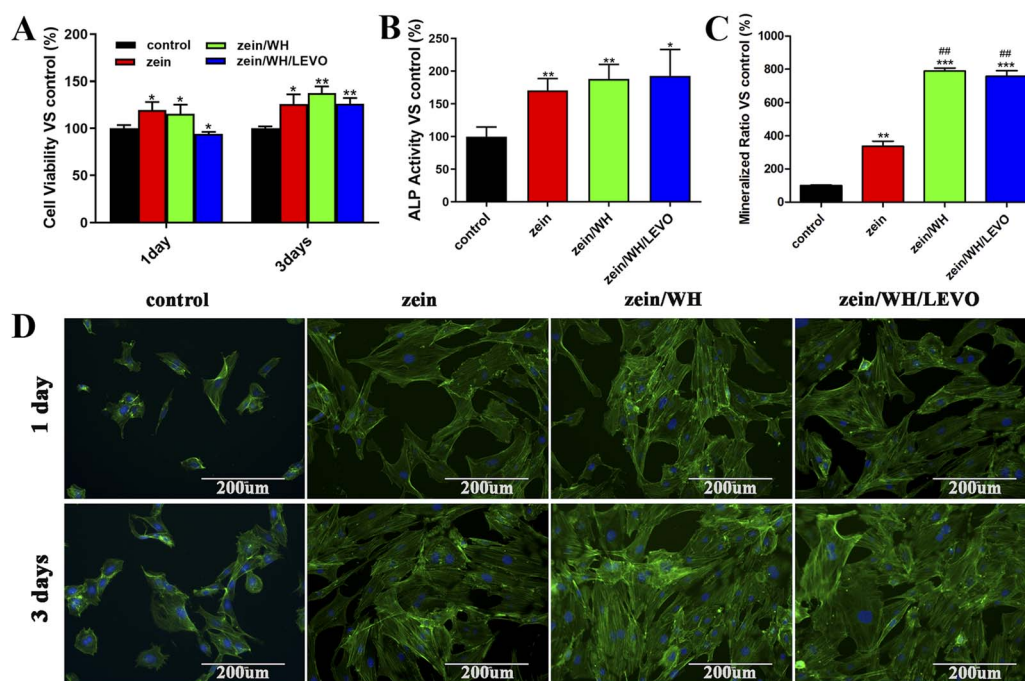


Fig. 4 The viability and differentiation of MC3T3-E1 cells on different scaffolds. (A) Cell viability; (B) ALP activity; (C) the mineralized matrix nodules; (D) fluorescence microscope images. *$p < 0.05$, **$p < 0.01$ and ***$p < 0.001$ for zein, zein/WH, zein/WH/LEVO *vs.* Control group; ##$p < 0.01$ for zein/WH, zein/WH/LEVO *vs.* zein group.

mineralization level on zein, zein/WH, and zein/WH/LEVO scaffolds exhibited a significant increase in comparison to the control group, indicating that three scaffolds can promote cell mineralization (Fig. 4C). Furthermore, the fluorescence microscope is used to observe the morphology of cells connected to scaffolds. The findings suggest that the surface of scaffolds provides a more favorable environment for cellular adhesion. At 1 day and 3 days, the cells on zein, zein/WH, and zein/WH/LEVO scaffolds have spread out and possess numerous filopodia compared to that of the control (Fig. 4D). It is indicated that the scaffolds can promote cell adhesion and stretch.

## 3.4.  The viability and angiogenesis of HUVECs

The osteogenic effect of scaffolds implantation depends on the degree of early vascularization. In addition, the new blood vessels can provide various components for osteogenic activities. In addition to essential nutrients, it also plays an indispensable role in the interaction between bone and neighboring tissues. The cell viability on scaffolds is quantified by the MTT method. The cell density on the scaffolds is comparatively higher than the control group at the time points of 1 day and 3 days (Fig. 5A). The experimental results indicate that three scaffolds have high biocompatibility without appreciable toxicity. The present investigation employed HUVECs as a cellular model to assess the angiogenic properties of the produced scaffolds. According to previous research, HUVECs

are considered to be a suitable and uniform experimental model due to their stable endothelial cell line.[39] The tube-like structure formation was observed to be enhanced on zein, zein/WH, and zein/WH/LEVO scaffolds, as compared to the control group (Fig. 5B). The analysis of quantitative data using Image J demonstrated a significant rise in the number of master junctions and meshes in comparison to the control group (Fig. 5C and D). The angiogenic effect of scaffolds may be related to the zein component in the scaffolds. The angiogenic effect of zein was mentioned in some references.[21,40] It may also be related to the $Mg^{2+}$ released from zein/WH and zein/WH/LEVO scaffolds. The $Mg^{2+}$ promotes the expression of platelet derived growth factor BB (PDGF-BB) secreted by precursor osteoclasts on the Src/JAK2 signaling pathway, then enhances its angiogenic effect.[41,42]

## 3.5.  Antibacterial property test

Infection is an important risk factor for bone repair. Bacterial or fungal infections can not only lead to bone repair failure but also increase the risk of treatment or secondary surgery.[43,44] As a third-generation quinolone drug, LEVO is widely used in severe infections of skin soft tissue, respiratory system, urinary system, and digestive system caused by sensitive bacteria.[45] LEVO was introduced into the scaffolds to prevent possible infection during bone repair. The antibacterial activity of zein, zein/WH, and zein/WH/LEVO scaffolds was investigated using
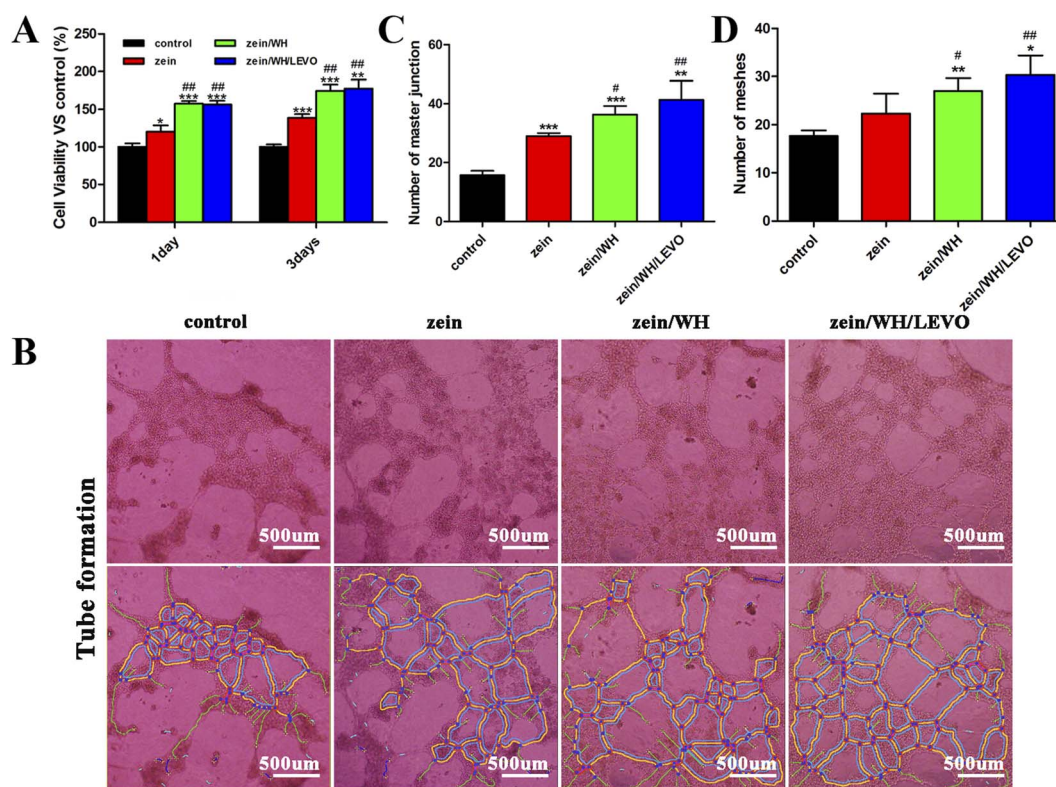


Fig. 5  The viability and angiogenesis of HUVECs on different scaffolds. (A) Cell viability; (B) microscopic images of cell tubular structure on different scaffolds; (C) number of master junction; (D) number of meshes. *$p < 0.05$, **$p < 0.01$ and ***$p < 0.001$ for zein, zein/WH, zein/WH/LEVO vs. Control group; #$p < 0.05$ and ##$p < 0.01$ for zein/WH, zein/WH/LEVO vs. zein group.

the agar disc diffusion method. It was found that zein/WH/LEVO scaffolds showed excellent antibacterial activity against MRSA with a zone of inhibition around 10 mm (Fig. S2†).

However, zein and zein/WH scaffolds have no bactericidal properties against bacterial strains. Thus, LEVO plays a decisive role in the antibacterial activity of composite scaffolds.
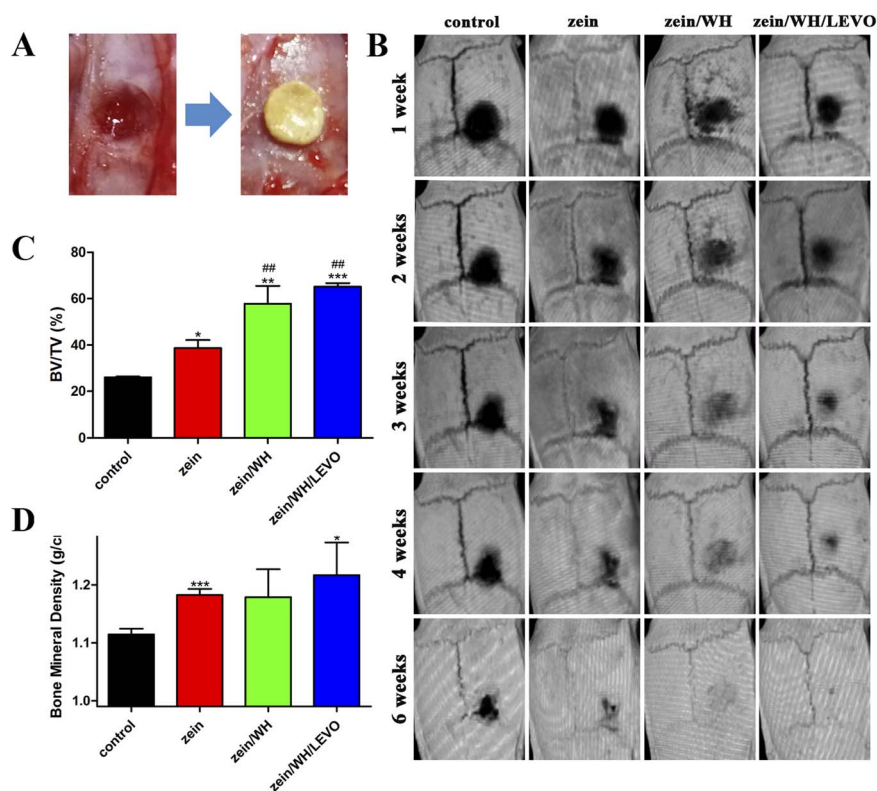


Fig. 6 The bone formation effects of different scaffolds *in vivo*. (A) The bone defect model; (B) micro-CT images of cranial defects after implantation of different scaffolds in rats; (C) BV/TV and (D) BMD of new bone formation after implantation of different scaffolds in rat for six weeks. *$p < 0.05$, **$p < 0.01$ and ***$p < 0.001$ for zein, zein/WH, zein/WH/LEVO *vs.* Control group; #$p < 0.05$ and ##$p < 0.01$ for zein/WH, zein/WH/LEVO *vs.* zein group.
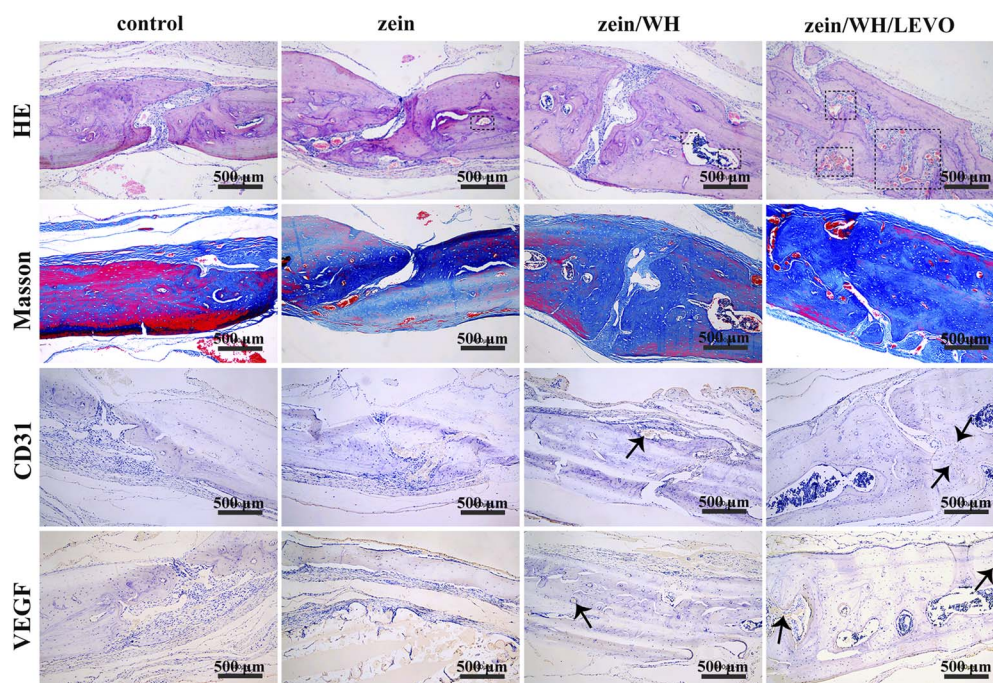


Fig. 7 Microscopic images of histomorphology and immunohistochemical of new bone formation after implantation for six weeks.

### 3.6. Bone formation analysis *in vivo*

Calvarial defects measuring 5 mm in diameter were induced in each rat using a trephine (Fig. 6A). At 1–6 weeks after surgery, the micro-CT images show the growth of new bone in the damaged bone area (Fig. 6B). The results demonstrate that the zein/WH/LEVO scaffolds promote new bone formation more effectively than the other groups at three, four, and six weeks. The micro-CT quantitative analysis reveals that the scaffolds composed of zein/WH/LEVO have the potential to improve the values of bone volume/tissue volume (BV/TV) and bone mineral density (BMD) at week six, as compared to the control and other groups (Fig. 6C and D). Based on the histomorphological and Masson images of bone sections, it is evident that the formation of bone tissue in the control group was comparatively inadequate in comparison to the zein group. However, the bone tissue in the zein/WH and zein/WH/LEVO group appeared to be relatively complete. The black dashed rectangle in the histomorphological staining images shows the formed bone tissue. The blue areas in the Masson staining images are the generated collagen fibers and skeletal muscle fibers (Fig. 7). The expression of VEGF and its receptor is a commonly used marker in angiogenesis. Research showed that etched titanium surfaces enhanced cell adhesion and increased VEGF expression, compared to that of control group.[46] Furthermore, the scaffolds for CD31 and VEGF had greater positive staining in contrast to the control group. The brown cells indicated by the black arrow in the images are positive expression cells (Fig. 7).

## 4. Conclusions

In this study, the zein/WH/LEVO composite scaffolds with good hydrophilicity and biocompatibility were synthesized successfully by salt leaching. The physical and chemical characterization results showed interconnected and porous scaffolds with presence of WH. The deposition of WH nanoparticles enhanced the tensile properties of the composite scaffolds. The composite scaffolds were found to promote cell migration, osteogenesis, and angiogenesis *in vitro* and *in vivo*. The incorporation of WH could result in a rise in osteoblast adhesion, differentiation, and mineralization. The osteoinductive and angiogenic effects of composite scaffolds may be related to the structure of scaffolds. LEVO plays a decisive role in the antibacterial activity of composite scaffolds. Using the three-dimensional microCT and histological analysis, it was found that the scaffolds can significantly promote bone repair in the rat skull defect model with the involvement of CD31 and VEGF. The results indicated the promising prospect of bone repair through tissue engineering. Thus, it is suggested that zein/WH/LEVO composite scaffolds would be used as a suitable material for bone regeneration.

## Author contributions

Xue Lin: investigation, methodology, data curation, writing – original draft. Yu Wang, Lingyu Liu and Xiaomeng Du: investigation, methodology. Shutao Guo: methodology. Wenying Wang: investigation, methodology. Jinchao Zhang: conceptualization, supervision. Kun Ge, Guoqiang Zhou: conceptualization, supervision, investigation, writing – review & editing, funding acquisition.

## Conflicts of interest

There are no conflicts to declare.

## Acknowledgements

## References

1 S. L. Teitelbaum, *Science*, 2000, **289**, 1504–1508.

2 X. Zhang, W. Jiang, C. Xie, X. Wu, Q. Ren, F. Wang, X. Shen, Y. Hong, H. Wu, Y. Liao, Y. Zhang, R. Liang, W. Sun, Y. Gu, T. Zhang, Y. Chen, W. Wei, S. Zhang, W. Zou and H. Ouyang, *Nat. Commun.*, 2022, **13**, 5211.

3 J. Zhang, D. Tong, H. Song, R. Ruan, Y. Sun, Y. Lin, J. Wang, L. Hou, J. Dai, J. Ding and H. Yang, *Adv. Mater.*, 2022, **34**, e2202044.

4 A. L. Farris, D. Lambrechts, Y. Zhou, N. Y. Zhang, N. Sarkar, M. C. Moorer, A. N. Rindone, E. L. Nyberg, A. Perdomo-Pantoja, S. J. Burris, K. Free, T. F. Witham, R. C. Riddle and W. L. Grayson, *Biomaterials*, 2022, **280**, 121318.

5 P. Lohmann, A. Willuweit, A. T. Neffe, S. Geisler, T. P. Gebauer, S. Beer, H. H. Coenen, H. Fischer, B. Hermanns-Sachweh, A. Lendlein, N. J. Shah, F. Kiessling and K. J. Langen, *Biomaterials*, 2017, **113**, 158–169.

6 D. I. Zeugolis, *Adv. Funct. Mater.*, 2020, **30**, 2005693.

7 D. Steiner, L. Reinhardt, L. Fischer, V. Popp, C. Körner, C. I. Geppert, T. Bäuerle, R. E. Horch and A. Arkudas, *Cells*, 2022, **11**, 926.

8 D. Campoccia, L. Montanaro and C. R. Arciola, *Biomaterials*, 2006, **27**, 2331–23339.

9 Y. Cui, H. Liu, Y. Tian, Y. Fan, S. Li, G. Wang, Y. Wang, C. Peng and D. Wu, *Mater. Today Bio*, 2022, **16**, 100409.

10 H. L. Jang, K. Jin, J. Lee, Y. Kim, S. H. Nahm, K. S. Hong and K. T. Nam, *ACS Nano*, 2014, **8**, 634–641.

11 A. Afonina, A. Kizalaite, A. Zarkov, A. Drabavicius, T. Goto, T. Sekino, A. Kareiva and I. Grigoraviciute-Puroniene, *Ceram. Int.*, 2022, **48**, 32125–32130.

12 H. D. Kim, H. L. Jang, H. Y. Ahn, H. K. Lee, J. Park, E. S. Lee, E. A. Lee, Y. H. Jeong, D. G. Kim, K. T. Nam and N. S. Hwang, *Biomaterials*, 2017, **112**, 31–43.

13 H. Cheng, R. Chabok, X. Guan, A. Chawla, Y. Li, A. Khademhosseini and H. L. Jang, *Acta Biomater.*, 2018, **69**, 342–351.

14 A. Dubey, S. Ghosh, S. Jaiswal, P. Roy and D. Lahiri, *Int. J. Biol. Macromol.*, 2022, **208**, 707–719.

15 M. Ma, W. He, X. Liu, Y. Zheng, J. Peng, Y. Xie, H. Meng and Y. Wang, *Composites, Part B*, 2022, **230**, 109533.

16 P. H. Tran and T. T. Tran, *Curr. Drug Targets*, 2020, **21**, 406–415.

17 I. Subuki, K. N. Ashikin Nasir and N. A. Ramlee, *Pertanika J. Sci. Technol.*, 2022, **30**, 2805–2829.

18 J. A. Tavares-Negrete, A. E. Aceves-Colin, D. C. Rivera-Flores, G. G. Díaz-Armas, A. S. Mertgen, P. A. Trinidad-Calderón, J. M. Olmos-Cordero, E. G. Gómez-López, E. Pérez-Carrillo, Z. J. Escobedo-Avellaneda, A. Tamayol, M. M. Alvarez and G. Trujillo-de Santiago, *ACS Biomater. Sci. Eng.*, 2021, **7**, 3964–3979.

19 S. Shrestha, B. K. Shrestha, S. W. Ko, R. Kandel, C. H. Park and C. S. Kim, *Carbohydr. Polym.*, 2021, **251**, 117035.

20 L. Polo, N. Gómez-Cerezo, A. García-Fernández, E. Aznar, J. L. Vivancos, D. Arcos, M. Vallet-Regí and R. Martínez-Máñez, *Chemistry*, 2018, **24**, 18944–18951.

21 H. J. Wang, S. J. Gong, Z. X. Lin, J. X. Fu, S. T. Xue, J. C. Huang and J. Y. Wang, *Biomaterials*, 2007, **28**, 3952–3964.

22 C. Qi, Y. J. Zhu, F. Chen and J. Wu, *J. Mater. Chem. B*, 2015, **3**, 7775–7786.

23 S. Gong, H. Wang, Q. Sun, S. T. Xue and J. Y. Wang, *Biomaterials*, 2006, **27**, 3793–3799.

24 S. Lin, L. Cui, G. Chen, J. Huang, Y. Yang, K. Zou, Y. Lai, X. Wang, L. Zou, T. Wu, J. C. Y. Cheng, G. Li, B. Wei and W. Y. W. Lee, *Biomaterials*, 2019, **196**, 109–121.

25 Y. Yuan, Q. Yuan, C. Wu, Z. Ding, X. Wang, G. Li, Z. Gu, L. Li and H. Xie, *ACS Biomater. Sci. Eng.*, 2019, **5**, 5872–5880.

26 S. Kandasamy, V. Narayanan and S. Sumathi, *Int. J. Biol. Macromol.*, 2020, **145**, 1018–1030.

27 L. Deng, D. Li, Z. Yang, X. Xie and P. Kang, *Biomed. Mater. Eng.*, 2017, **28**, 361–377.

28 J. Wang, Y. Liu, G. Lin, H. Chang, Y. Li, Y. Yang, H. Matsuyama, B. Lee, Y. Chen and K. Tung, *Surf. Coat. Technol.*, 2020, **386**, 125452.

29 M. Babaei, A. Ghaee and J. Nourmohammadi, *Mater. Sci. Eng., C*, 2019, **100**, 874–885.

30 J. Zhang, H. Zhou, K. Yang, Y. Yuan and C. Liu, *Biomaterials*, 2013, **34**, 9381–9392.

31 M. Demir, L. Ramos-Rivera, R. Silva, S. NNazhat and A. R. Boccaccini, *J. Biomed. Mater. Res., Part A*, 2017, **105**, 1656–1665.

32 J. Y. Ru, Q. Wei, L. Q. Yang, J. Qin, L. C. Tang, J. Wei, L. P. Guo and Y. F. Niu, *RSC Adv.*, 2018, **8**, 18745–18756.

33 Y. Q. Xue, Y. C. Zhang, Y. B. Zhang and J. Y. Wang, *Biomed. Eng. Adv.*, 2023, **5**, 100059.

34 S. J. Li, L. Y. Zhang, C. Y. Liu, J. Kim, K. Su, T. L. Chen, L. M Zhao, X. M. Lu, H. Zhang, Y. L. Cui, X. Cui, F. Yuan and H. B. Pan, *Bioact. Mater.*, 2023, **23**, 101–117.

35 G. Labib, *Expert Opin. Drug Delivery*, 2018, **15**, 65–75.

36 Z. Shahbazarab, A. Teimouri, A. N. Chermahini and M. Azadi, *Int. J. Biol. Macromol.*, 2018, **108**, 1017–1027.

37 H. Lian, X. Liu and Z. X. Meng, *J. Mater. Sci.*, 2019, **54**, 719–729.

38 Z. Shahbazarab, A. Teimouri, A. N. Chermahini and M. Azadi, *Int. J. Biol. Macromol.*, 2017, **108**, 1017–1027.

39 W. J. Yang, J. B. Yan, L. Zhang, F. Zhao, Z. M. Mei, Y. N. Yang, Y. Xiang and Y. Q. Xing, *Exp. Ther. Med.*, 2020, **20**, 901–909.

40 H. J. Wang, J. C. Huang, L. Hou, T. Miyazawa and J. Y. Wang, *J. Mater. Sci.: Mater. Med.*, 2016, **27**, 92.

41 W. Liu, S. Guo, Z. Tang, X. Wei, P. Gao, N. Wang, X. K. Li and Z. Guo, *Biochem. Biophys. Res. Commun.*, 2020, **528**, 664–670.

42 H. Xie, Z. Cui, L. Wang, Z. Xia, Y. Hu, L. L. Xian, C. J. Li, L. Xie, J. Crane, M. Wan, G. H. Zhen, Q. Bian, B. Yu, W. Z. Chang, T. Qiu, M. Pickarski, L. T. Duong, J. J. Windle, X. H. Luo, E. Y. Liao and X. Cao, *Nat. Med.*, 2014, **20**, 1270–1278.

43 J. L. Paris, N. Lafuente-Gómez, M. V. Cabañas, J. Román, J. Peña and M. Vallet-Regí, *Acta Biomater.*, 2019, **86**, 441–449.

44 H. Sun, C. Hu, C. Zhou, L. Wu, J. Sun, X. Zhou, F. Xing, C. Long, Q. Kong, J. Liang, Y. Fan and X. Zhang, *Mater. Des.*, 2020, **189**, 108540.

45 M. Meléndez-Carmona, I. Muñoz-Gallego, E. Viedma, J. Lora-Tamayo and F. Chaves, *Int. J. Antimicrob. Agents*, 2019, **54**, 356–360.

46 G. D. Marconi, F. Diomede, J. Pizzicannella, L. Fonticoli, I. Merciaro, S. D. Pierdomenico, E. Mazzon, A. Piattelli and O. Trubiani, *Cell Dev. Biol.*, 2020, **8**, 315.